Desalination and Water Treatment
www.deswater.com

doi: 10.5004/dwt.2022.28910

276 (2022) 150–159
November

Removal of Ni(II) ions from aqueous solutions with Siirt Koçpınar mixed type clay investigation of isotherm, thermodynamic and kinetic parameters

Nilgün Onursal

Department of Primary Education, Faculty of Teachers College, Siirt University, Siirt, Turkey, Tel. +90 5055808493; email: nilgun.onursal@gmail.com

Received 10 May 2022; Accepted 3 September 2022

ABSTRACT

This study used mixed-type clay as an adsorbent to remove Ni(II) ions from the aqueous solution. Crystallographic analyses were performed for crystalloplotic identification. Concentration, temperature, amount of adsorbent, and thermodynamic parameters, which are among the parameters affecting the adsorption, were examined. The obtained data were applied to the Freundlich, Langmuir, Temkin, and Dubinin–Radushkevich adsorption isotherms. It was determined that the data fit the Langmuir adsorption isotherm model the most. The adsorption capacities were determined as 24.81, 29.85 and 58.14 mg/g Ni on clay at 298, 308, and 313 K, respectively. Kinetics data were obeyed to pseudo-second-order. Thermodynamic data (for 298, 308, and 318 K) were calculated as ΔG = –18.569, –20.879, –23.189 kJ/mol, ΔH = 22.60 kJ/mol and ΔS = 0.141 kJ/mol·K, respectively. The ΔH and ΔS values can be obtained directly from the slope and shift of the Gibbs plot presented in this study which is not seen before in the literature. The clay used in the study was chosen due to its low cost and easy acquisition, and as a result of the analysis, it was determined that it could be used as an adsorbent with moderate efficiency in removing Ni(II) ions from water.

Keywords: Adsorption; Isotherm; Kinetics; Thermodynamics; Nickel; Clay

1. Introduction

The adsorption process has recently played an important role in water and wastewater treatment thanks to solid–liquid adsorption. The adsorption process is used for many purposes in water and wastewater treatment [1]. As the metal usage in the rapidly developing industries increases, the damage to the environment and nature caused by the aforementioned usage increases parallelly. Everyone accepts the carcinogenic effect of heavy metals. Heavy metals are considered a severe pollution source. While heavy metals participate in biological reactions in trace amounts, they can negatively affect vital functions if they are to be found in more than the necessary amount in the body. In addition to its meaning of rock, the term clay is a concept that expresses the particle size, that is, the coarseness of the particle according to the results of the mechanical analysis of soil and sedimentary rocks. Wentworth proposed in 1922 to call the particles smaller than 4 microns (1/256 mm) clay according to chemical classification [2,3]. We can define clays as aluminosilicates [4].

Some usage areas of clay minerals are; cement, brick, tile, structural tile, floor tile, tile, sewer pipe, drainage pipes, sewage pipe, sanitary ware, filling, drilling, coatings (asphalt, etc.), pottery, tile, glass, porcelain, electro porcelain, refractory industries and for casting industry clay is an essential material, especially in terms of chemistry and mineralogy. Clay's physical and chemical properties determine its adsorbing identity.

In the current century, time is moving faster, so its significance has increased. Accordingly, kinetics' and its sub-discipline adsorption kinetics' significance also increase. Thus, the number of scientific studies on this subject is increasing

daily. Therefore, it would be suitable to mention two points about adsorption at this point: firstly, a slow-moving process has no economic value. For example, if the adsorption method is used to pre-treatment a pool or city water, a slow adsorption rate will mean service disruption. Secondly, whether the adsorption time is long or short will give us some scientific ideas. For example, adsorption that equilibrates quickly indicates that the affinity between the adsorbent and the adsorbed is good. Numerous models have been proposed to explain the adsorption kinetics. The most well-known ones are the pseudo-first-order kinetic model, [5] pseudo-second-order kinetic model, intraparticle diffusion model, and Elovich kinetic model.

The formulas and explanations related to the kinetic models mentioned above are given in Table 1.

Adsorption is the process of deposition of matter from the liquid or gas phase to the surface of the solid phase. Many isotherm models identify the interaction between adsorbate and adsorbent molecules. The Table 2 gives information about the isotherm models widely used in the literature.

2. Materials and methods

The used material (Merck Trademark, USA) $NiN_2O_6{\cdot}3H_2O$ is analytical grade. The used Siirt Koçpınar

Table 1
Adsorption kinetic models and equations

Kinetic model – Formula	Explanation
Pseudo-first-order $\log\left(q_e - q_t\right) = \log q_e - kt$	where k_1 is the first-order rate constant of adsorption; q_e indicates the amount of substance adsorbed at equilibrium, and q_t indicates the amount of substance adsorbed at the end of time (t) [6–9]. In this case, q_e and q_t are the amounts of adsorbed material at equilibrium and time t (min), and k_1 is the rate constant of adsorption (min^{-1}), respectively [10–12].
Pseudo-second-order $\frac{t}{q_t} = \frac{1}{k_2 q_e^2} + \left(\frac{1}{q_e}\right)t$	This model is based on the assumption that adsorption can be chemical. In the equation, k_2 (g/mg·min) is the second-order rate [13,14].
Weber and Morris (intraparticle diffusion model) $q_t = k\sqrt{t} + C$	The intraparticle model is widely applied to study as the rate-limiting step during adsorption. Adsorption of the solute in a solution includes adsorbate mass migration, surface diffusion, and pore diffusion. k is the rate constant mg/g·$min^{1/2}$, and C is the boundary layer thickness. The values of C presents the boundary layer effect [15].
Elovich kinetic model $q_t = \frac{1}{\beta}\ln\left(\alpha\beta\right) + \frac{1}{\beta}\ln t$	This model assumes that the adsorption rate of the solute decreases exponentially as the amount of adsorbed material increases [16].

Table 2
Adsorption isotherm models and equations

Isotherm model – Formula	Explanations
Freundlich $\log q_e = \log K_F + \frac{1}{n}\log C_e$	According to the Freundlich model, the adsorption sites on the surface of an adsorbent have a heterogeneous structure. It consists of different types of adsorption sites. The linearized Freundlich expression is given in the equation on the left [17,18,19].
Langmuir $\frac{C_e}{q_e} = \frac{C_e}{q_{\max}} + \frac{1}{K_L q_m}$	The mathematical expression of the linearized Langmuir model is given on the left side. Where; K_L: Langmuir constant (L/mg) [20].
Dubinin–Radushkevich (D-R) model $\ln q_e = \ln q_m - \ln q\beta\varepsilon^2$ $E = -\frac{1}{\sqrt{\beta}}$	Dubinin–Radushkevich: It is used to characterize the adsorption curve according to the pore structure of the adsorbent. R is gas constant (8.314 J/mol·K), T is the absolute temperature (K), β isotherm constant related to adsorption energy, q_m is theoretical adsorption capacity, and ε is Polanyi potential. The average adsorption energy (E) helps us to predict the adsorption mechanism. For example, if the E value is 8–16 kJ/mol, the adsorption process is characterized by ion-exchange, if E < 8 kJ/mol, the adsorption is physical [21].
Temkin model $\ln q_e = B_T \ln K_T + B_T \ln C_e$	In this isotherm, the enthalpy of adsorption calculation is developed for all molecules present in the solution while considering the interactions between the adsorbed substances. The B value is the constant related to the heat of adsorption (J/mol) and is expressed as $B_T = RT/b$. b is the Temkin isotherm constant. T is the absolute temperature (K). R is the ideal gas constant (J/mol·K) [22].

mixed type clay (SKMTC) as adsorbent was supplied from Koçpınar Village-Siirt, Turkey. The clay was dried, grounded, sieved, and then characterized by X-ray diffraction (XRD), X-ray fluorescence (XRF), Fourier-transform infrared spectroscopy (FT-IR), scanning electron microscopy-energy-dispersive X-ray spectroscopy (SEM-EDX), Brunauer–Emmett–Teller (BET) methods. The XRD analysis of the clay was performed with the Bruker D8 Advance XRD analyzer (4-700 detail clay) with Cu-X-ray tube, and the quantitative analysis was performed using the Rietveld (1969) method using the PANalytical X'Pert highscore plus program and the ICSD database. The multipoint surface area and pore size determination analysis of the sample was carried out thanks to BET method. Vacuum treatment was applied to the sample at 77.3 K temperature for 23 h. Adsorption experiments were carried out in two groups as equilibrium and kinetic. The study was carried out at 298, 308, and 318 K temperatures. The amount of nickel remaining in the solution was analyzed using the atomic absorption spectroscopy (AAS) instrument. The values of q_e and q_t were calculated using Eqs. (1) and (2).

In order to determine the chemical composition of the adsorbent, the samples were dried at 105°C for XRF analysis, and the analysis results were obtained thanks to the UQ program of Thermo ARL brand XRF device. FT-IR analysis was conducted with Agilent Cary 630 brand device. Field-emission scanning electron microscopy (FESEM-EDX) analysis was performed-both before and after the experiment with Quanta FEG-250 model device to determine the changes occurred due to the presence of nickel in the adsorbent.

$$q_e = \frac{(C_i - C_e)V}{m} \tag{1}$$

$$q_t = \frac{(C_i - C_t)V}{m} \tag{2}$$

where q_e; the amount of substance adsorbed in equilibrium (mg/g), q_t; the amount of substance adsorbed at any time t (mg/g), C_i; initial concentration (mg/L), C_e; its concentration at equilibrium (mg/L). C_t; instantaneous concentration (mg/L), V; the solution volume (L) and m; the amount of adsorbent material (g).

2.1. Discussions and result

2.1.1. XRD analysis

In Table 3, clay XRD values of SKMTC and detailed clay XRD values are given. In the Table 3, the general mineral composition of SKMTC in the detailed XRD data, and the results of qualitative detailed XRD analysis of clay are presented as the enrichment process for the clay group minerals that cannot be identified by standard analysis.

In the XRD clay analysis, since quartz and calcite constitute more than 50% of the clay, the main elements of the clay are neglected; however, in the detailed XRD analysis of the clay, the ratio of muscovite illite and vermiculite can be selected more clearly since clay is purified from quartz and calcite.

2.1.2. XRF analysis

XRF analysis of clay is given in Table 4. According to the XRF analysis of clay, the % presence of elemental oxides is respectively;

$SiO_2 > CaO > MnO > Al_2O_3 > Fe_2O_3 > MgO > K_2O > TiO_2 > Na_2O > P_2O_6 = MnO$

2.1.3. BET analysis

The specific surface area of the clay used as adsorbent was measured as (BET = 19.178 m^2/g). Total pore volume of pores with radius was measured less than 0.1 μm at P/P_o. The average pore radius was measured as 4.334×10^{-3} μm. Table 5 is the BET characterization table.

2.1.4. FT-IR analysis

FT-IR analysis results are given before the experiment in Fig. 1a and after the experiment in Fig. 1b. When the FT-IR spectrum is examined, the peaks at 3,566.06 and 3,616.37 displays –OH stretching peaks, the peaks at 1,433.70 and 1,434.74 cm^{-1} displays due to calcite in clay the presence of CO_3^{2-} and the peak at 976.90 and 999.12 cm^{-1} displays Si–O bond. The peaks at 872.42, 711.99 and 712.09 cm^{-1} belong to the O–C–O asymmetric vibration motion. The adsorption

Table 3
XRD data and detailed XRD data of SKMTC

Name	Clay XRD values %	Clay detail XRD values %
Muscovite	12	25
Calcite	35	–
Montmorillonite	6	12
Quartz	17	–
Chloride	6	12
Kaolinite	7	15
Illite	9	19
Vermiculite	8	17

Table 4
XRF values of SKMTC (%)

Sample	K.Ç.P./Aynbaran
A.Za	21.80
AL_2O_3	11.5
CaO	22.3
Fe_2O_3	5.4
K_2O	1.8
MgO	2.5
MnO	0.1
Na_2O	0.4
P_2O_6	0.1
SiO_2	32.9
TiO_2	0.6

Table 5
BET characterization table

Surface area data	
Multipoint BET	1.918e+01 m^2/g
BJH method cumulative adsorption surface area	8.650e+00 m^2/g
BJH method cumulative desorption surface area	1.445e+01 m^2/g
DH method cumulative adsorption surface area	8.798e+00 m^2/g
DH method cumulative desorption surface area	1.469e+01 m^2/g
1-method external surface area	1.380e+01 m^2/g
1-method micropore surface area	5.379e+00 m^2/g
NLDFT cumulative surface area	1.586e+01 m^2/g
Pore volume data	
Total pore volume for pores with radius less than 0.10 μm at P/P_o = 0.990345	4.154e-02 cc/g
BJH method cumulative adsorption pore volume	3.581e-02 cc/g
BJH method cumulative desorption pore volume	3.587e-02 cc/g
DH method cumulative adsorption pore volume	3.488e-02 cc/g
DH method cumulative desorption pore volume	3.497e-02 cc/g
1-method micropore volume	2.529e-03 cc/g
HK method cumulative pore volume	1.109e-02 cc/g
SF method cumulative pore volume	1.112e-02 cc/g
NLDFT cumulative pore volume	3.181e-02 cc/g
Pore size data	
Average pore radius	4.332w-03 μm
BJH method adsorption pore radius (mode Dv(r))	1.524e-03 μm
BJH method desorption pore radius (mode Dv(r))	1.867e-03 μm
DH method adsorption pore radius (mode Dv(r))	1.524e-03 μm
DH method desorption pore radius (mode Dv(r))	1.867e+01 μm
HK method pore radius (mode)	2.158e-04 μm
SF method pore radius (mode)	1.754e-04 μm
NLDFT pore radius (mode)	1.385e-03 μm

peak at 797.84 and 798.63 cm^{-1} is attributed to Si(AI)–O and Si–O–Si (AI) [23].

2.1.5. FESEM-EDX analysis

In Fig. 2 the images of SKMTC in its natural state are seen in close and long shots. In the image taken after the interaction between metal and clay, as seen in Fig. 3, the images display that the shines are formed and hold the metal. In Fig. 4. EDX diagram of natural clay – according to FESEM image of the clay – is presented.

As a result of the SEM-EDX analysis performed after the experiment, the presence of nickel around 0.85 keV is observed.

2.2. Experimental findings

2.2.1. Isotherm studies

Isotherm curves are obtained when the remaining substance is plotted against the amount of adsorbed substance. As seen in Fig. 6, it is observed that the adsorption increases as the temperature increases. The adsorption data obtained in this study were applied to the linear isotherms of Freundlich, Langmuir, Temkin, and Dubinin–Radushkevich. Plot of these models are given in Figs. 6 and 7.

The effects of factors such as concentration, amount of adsorbent, time, and temperature on the adsorption of Ni(II) ions on natural clay were investigated in the experimental study. One of the aims of this study is to determine the optimum conditions for the adsorption of Ni(II) metal ions. Parameters obtained from the plots are given in Table 6.

When the data given in Table 7 are compared, it is clearly seen that the adsorption capacity of SKMTC is higher than the other clays.

2.3. Thermodynamic calculations

Based on the k_d values obtained from the experimental studies, the van't Hoff plot was created. ΔH and ΔS values were calculated by writing the parameters obtained from the plot in their places in Eq. (3). These values were replaced in Eq. (4), and ΔG values were found for each temperature. The values found are given in Table 7.

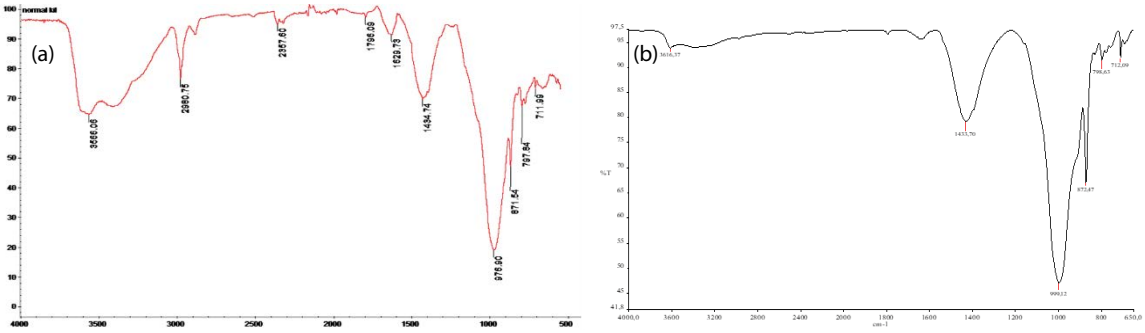

Fig. 1. FT-IR diagram (a) of natural clay and (b) after clay interacts with metal.

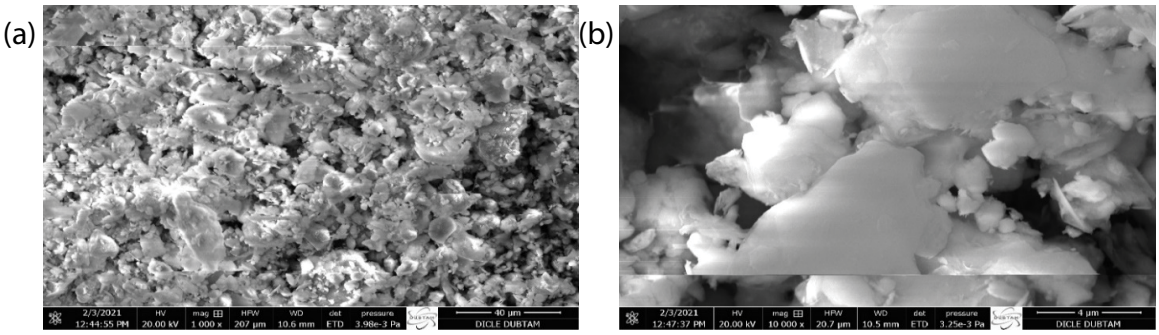

Fig. 2. FESEM images of (a) natural clay (long shot) and (b) natural clay (close shot).

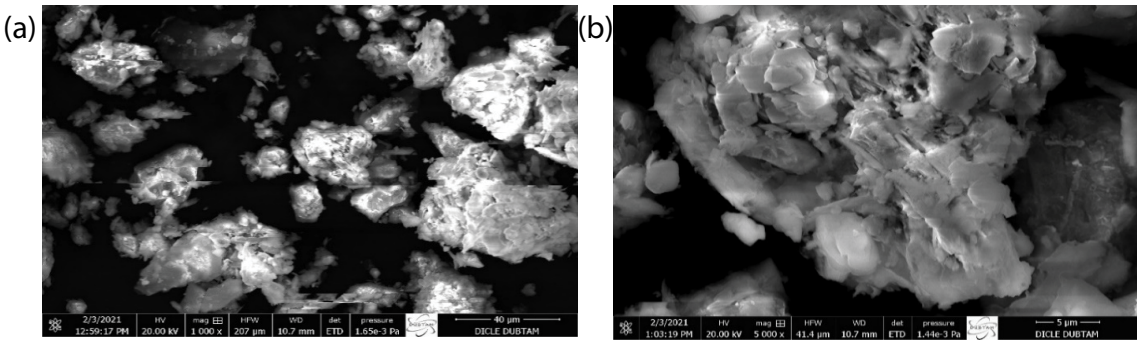

Fig. 3. FESEM images (a) after clay interacts and (b) clay interacts with metal (long shot) with metal (close shot).

$$\ln k_d^0 = -\frac{\Delta H}{RT} + \frac{\Delta S}{R} \tag{3}$$

$$\Delta G = \Delta H - T\Delta S \tag{4}$$

where k_d represents the adsorption equilibrium constant, ΔG represents the Gibbs free energy change resulting from adsorption, ΔH represents the adsorption enthalpy change, ΔS represents the entropy change, and T represents the absolute temperature. Kinetics, on the other hand, by its nature, examines the situation before it comes to dynamic equilibrium.

The obtained $\ln k_d^0$ values were placed in Eq. (3), and the van't Hoff plot in Fig. 9 was obtained from the slope.

The ΔH value was found from the slope of the van't Hoff plot and the ΔS value from the shear. These values were placed in Eq. (4), and ΔG values were found for each temperature.

Gibbs plot presenting the terms of adsorption thermodynamics is given in Fig. 10. The adsorption ΔH can be seen from the slope of the graph without the need for any calculations. The negative value of the shift of the graph equation presents ΔH; on the other hand, the shift of the equation presents entropy.

As it is presented in Table 8, the negative values of ΔG show that the adsorption phenomenon occurs spontaneously. In addition, a positive ΔH value indicates that the event is endothermic. The fact that the ΔH value is greater than 40 kJ/mol is a great proof that the adsorption is chemical. The fact that the experimental results are mostly compatible with the Langmuir model also indicates that the phenomenon is chemical.

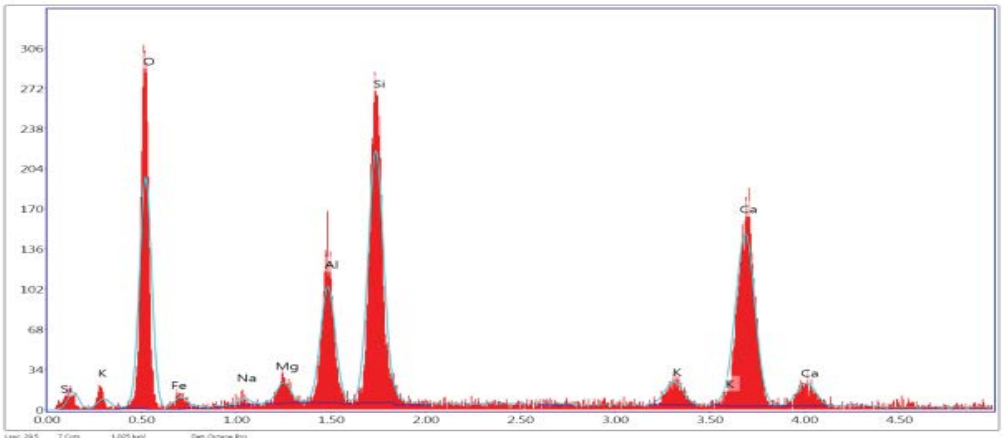

Element	Wt %	Atomic %	Error %	Net Int.	Net Error %	K Ratio	Z	R	A	F
O K	51.84	69.15	10.91	103.09	2.27	0.1218	1.0607	0.9643	0.2216	1.0000
Fe L	5.04	1.93	27.50	3.08	19.28	0.0113	0.8333	1.1185	0.2706	0.9971
Na K	0.85	0.79	71.20	3.09	63.43	0.0025	0.9649	0.9912	0.3044	1.0042
Mg K	1.49	1.31	22.40	10.38	15.97	0.0067	0.9818	0.9990	0.4530	1.0075
Al K	7.06	5.58	8.93	62.35	3.89	0.0399	0.9458	1.0063	0.5925	1.0100
Si K	14.32	10.88	6.72	140.79	2.39	0.0923	0.9668	1.0132	0.6619	1.0074
K K	1.88	1.03	16.20	15.82	14.20	0.0167	0.8973	1.0424	0.9334	1.0630
Ca K	17.52	9.33	4.38	121.60	2.78	0.1548	0.9138	1.0473	0.9525	1.0152

Fig. 4. EDX diagram obtained as a result of the interaction of natural clay.

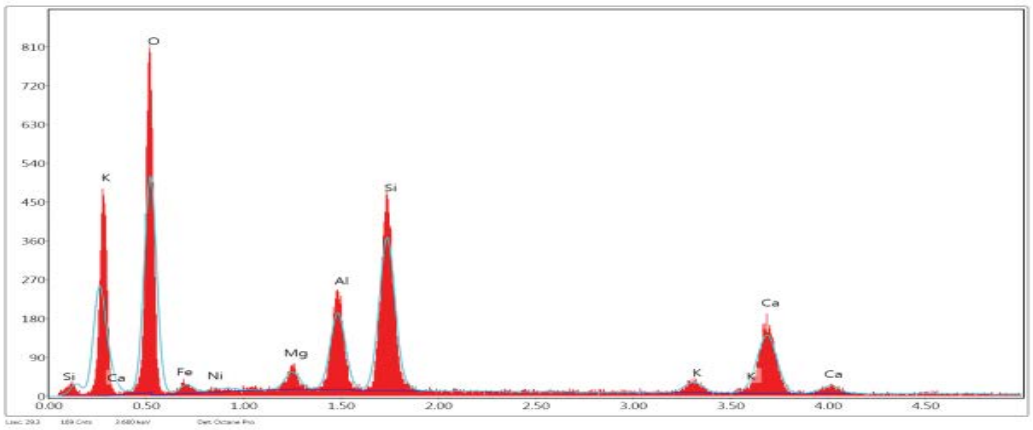

Element	Wt %	Atomic %	Error %	Net Int.	Net Error %	K Ratio	Z	R	A	F
O K	51.71	69.05	9.38	267.24	1.49	0.1810	1.0691	0.9652	0.3274	1.0000
Mg K	1.89	1.66	16.01	24.42	10.64	0.0110	0.9822	0.9989	0.5889	1.0076
Al K	7.77	6.15	7.22	113.31	3.03	0.0526	0.9448	1.0059	0.7105	1.0099
Si K	15.58	11.85	5.55	235.32	1.88	0.1155	0.9645	1.0125	0.7633	1.0066
K K	1.99	1.09	17.39	19.58	15.21	0.0179	0.8896	1.0392	0.9567	1.0562
Ca K	14.33	7.64	5.72	112.92	3.78	0.1283	0.9048	1.0433	0.9694	1.0209
Fe K	5.62	2.15	21.18	16.50	18.68	0.0478	0.7985	1.0553	0.9963	1.0690
Ni K	1.11	0.41	61.84	2.19	58.85	0.0097	0.8005	1.0515	0.9974	1.0923

Fig. 5. EDX diagram of nickel(II) ions adsorbed the clay.

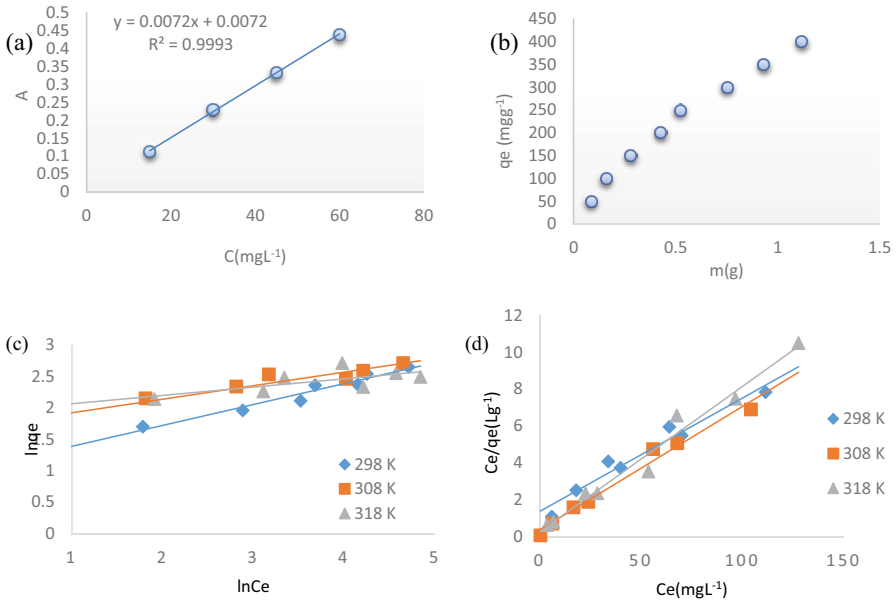

Fig. 6. (a) Calibration plot of Ni(II) for different temperatures, (b) effect of adsorbent amount on Ni(II) adsorption, (c) Freundlich plot of Ni(II) and (d) Langmuir plot of Ni(II).

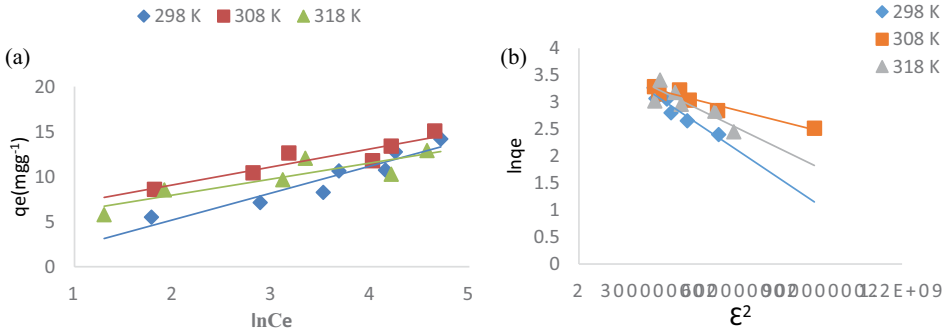

Fig. 7. For different temperatures: (a) Temkin Plot of Ni(II) and (b) D-R Plot of Ni(II).

Table 6
Parameters obtained adsorption concentration experiments

	Langmuir isotherm			Freundlich isotherm		Temkin isotherm			Dubinin–Radushkevich isotherm			
T (K)	K_L (L/mg)	q_{max} (mg/g)	R^2	K_F	n	R^2	B	K_{TM}	R^2	K_{DR} (L/mg)	E (kJ/mol)	R^2
298	0.114	24.81	0.8969	2.879	1.69	0.9457	2.9836	0.019	0.8955	-3×10^{-9}	12.9	0.7678
308	0.182	29.85	0.9807	4.910	1.60	0.7708	1.9982	1.489	0.8490	1×10^{-9}	22.36	0.9294
318	0.297	25.38	0.9753	5.364	1.76	0.7868	1.7803	1.208	0.7833	2×10^{-9}	15.81	0.7485

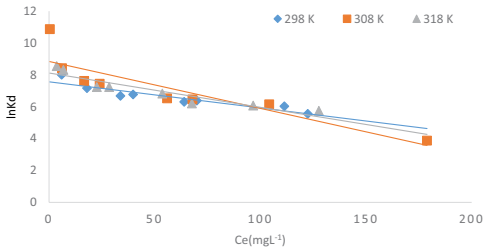

Fig. 8. lnK_d plot of different concentration values of Ni(II) at different temperatures.

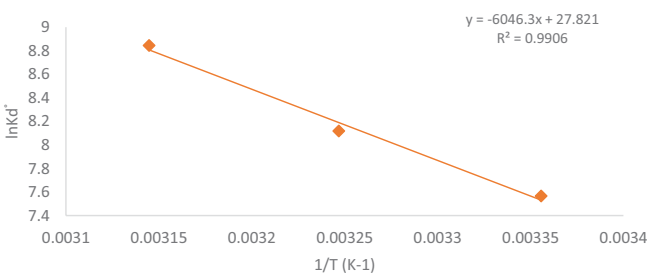

Fig. 9. Van't Hoff plot of Ni(II).

Table 7
Comparison adsorption capacities with SKMTC and other clays

Adsorbent	Adsorption capacity (mg/g)	Reference
Raw kaolinite	6.21	[24]
Kaolinite	20.49	[25]
Fibrous clay minerals	85	
Clay	6.3	[26]
Natural clay	15.4	
Surfactant-modified clay	0.24	[27]
SKMTC	29.85	This study

Table 8.
Thermodynamic data adsorption of Ni(II) metal on SKMTC

T (K)	$1/T$	$\ln k_d^0$	ΔG (kJ/mol)	ΔH (kJ/mol)	ΔS (kJ/mol·K)
298	3.36×10^{-3}	7.5652	–18.569		
308	3.25×10^{-3}	8.1174	–20.879	50.269	0.231
318	3.14×10^{-3}	8.8436	–23.189		

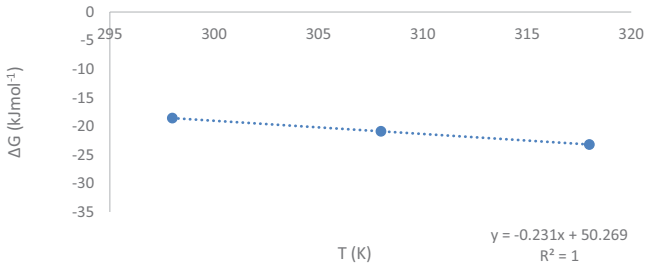

Fig. 10. Gibbs plot of Ni(II) on SKMTC.

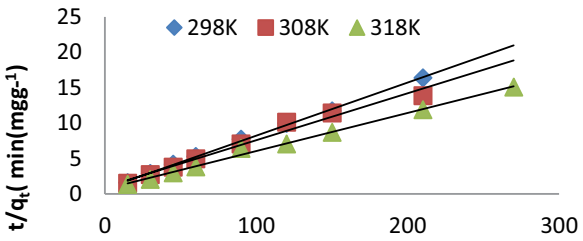

Fig. 12. Pseudo-second-order plot of Ni(II) at different temperatures.

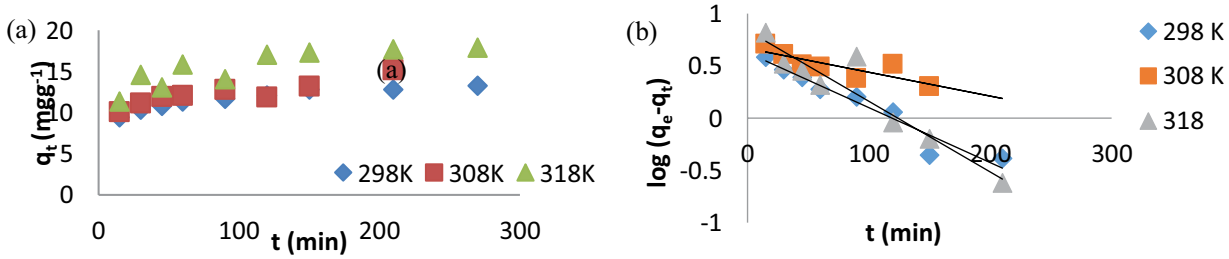

Fig. 11. For different temperatures: (a) effect of adsorption contact time and (b) pseudo-first-order of Ni(II) on SKMTC.

Table 9.
Constants achieved from adsorption kinetic experiment

	Pseudo-first-order			Pseudo-second-order			Elovich model			Weber–Morris model		
T (K)	k_1 (dk^1)	q_e	R^2	K	q_e (mg/g)	R^2	β	α	R^2	K_i (mg/g·dk$^{1/2}$)	C (mg/g)	R^2
298	0.0053	4.223	0.9403	0.0078	13.333	0.9985	0.7457	96.873	0.9842	0.2942	8.7283	0.9457
308	0.0023	4.645	0.6989	0.0046	15.083	0.9782	0.6538	69.06	0.8016	0.3838	8.8575	0.8372
318	0.0068	7.798	0.8922	0.0043	18.587	0.9947	0.4901	55.735	0.8238	0.4392	11.357	0.7542

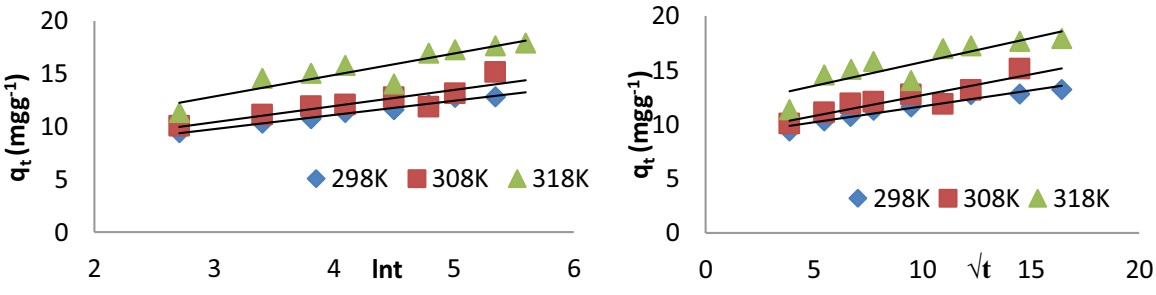

Fig. 13. For different temperatures: (a) Elovich and (b) Weber–Morris plot Ni(II) on SKMTC.

2.4. Kinetic studies

Adsorption is a time-dependent process. In adsorption kinetics, there is an equilibrium contact time between the adsorber and the adsorbed. Equilibrium contact time is while the adsorbent is saturated with the adsorbed [28,29]. In kinetic studies, regression analyses of models are often performed. It is found by comparing the model most suitable for the experimental data. This study investigated the suitability of pseudo-first-order, pseudo-second-order, Weber–Morris, and Elovich kinetic models at 298, 308, and 318 K. Kinetic plots were created with the values obtained from the kinetic studies' data at all three temperatures. The parameters obtained from these plots are presented in Table 9.

3. Conclusion

The adsorption amount, temperature, and concentration parameters were examined in the study. Data from experimental studies were applied to Langmuir, Freundlich, Temkin, and Dubinin–Radushkevich models. When the obtained data were compared, it was determined that the result was compatible with the Langmuir isotherm. The adsorption capacities, q_m, were determined as 24.81, 29.85, and 58.14 mg/g Ni on clay at 298, 308, and 313 K, respectively. The kinetic study data were applied to pseudo-first-order, pseudo-second-order, Elovich, and intraparticle diffusion models. It was determined that the data fit the pseudo-second-order kinetic model the most. q_e values were determined as 13.333, 15.083 and 18.587 mg/g Ni on clay at 298, 308, and 313 K, respectively. Thermodynamic ΔH and ΔS values were found as 22.599 kJ/mol, 0.141 kJ/mol·K, and ΔG values for 298, 308 and 318 K were found as –18.569, –20.879, and –23.189 kJ/mol, respectively. The results show that adsorption is an endothermic and spontaneous process. In the Gibbs plot presented in this study, which has not been seen before in the literature; the ΔH and ΔS values can be found directly from the slope and shift of the plot. The least-squares method (R^2) was used for the regression analysis of the kinetic study. According to this, it was determined that the adsorption kinetics realized at 298 K temperature complied with all models, and at 308K and 318 K temperatures, results complied with all models except the pseudo-second-order kinetic model. The amount of substance adsorbed at equilibrium, q_e was determined as 13.333, 15.083 and 18.587 mg/g, 298, 308, and 318 K, respectively. It has been determined that the clay used in the adsorption process is a suitable adsorbent, and its cheapness and abundance make its usage advantageous compared to other clays in the literature.

References

[1] EPA, Primer for Municipal Wastewater Treatment Systems, United States Environmental Protection Agency, USA, Washington, 2004.

[2] N.R. O'Brien, R.M. Slatt, Introduction, in: Argillaceous Rock Atlas, Springer, New York, 1990. Available at: https://doi.org/10.1007/978-1-4612-3422-7_1

[3] H.L. Alling, A metric grade scale for sedimentary rocks, J. Geol., 51 (1943) 259–269.

[4] J.M. Huggett, Clay Minerals, Encyclopedia of Geology, 2005, pp. 358–365.

[5] H. Elik, A.R. Kul, V. Benek, Van pomzası üzerinde kurşun iyonunun adsorpsiyon 29, Ulusal Kimya Kongresi, Erciyes Üniversitesi Fen Bilimleri Enstitüsü, 2019, p. 62. (Adsorption of Lead Ion on Van Pumice 29th National Chemistry Congress, Erciyes University Institute of Science and Technology, 2019, p. 62).

[6] M.F. Baran, M.Z. Duz, Removal of cadmium(II) in the aqueous solutions by biosorption of *Bacillus licheniformis* isolated from soil in the area of Tigris River, Int. J. Environ. Anal. Chem., 101 (2021) 533–548.

[7] M.C. Dal, N. Onursal, E. Arıca, Ö. Yavuz, Diyarbakır Karacadağ Kırmızı Tepe Skoryası ile Cu(II)'nin adsorpsiyon kinetiğinin incelenmesi, Dümf Mühendislik Dergisi, 12 (2021) 337–346. (Investigation of the adsorption kinetics of Cu(II) with Diyarbakır Karacadag Kırmızı Tepe Scoria, DUJE, 12 (2021) 337–346).

[8] D. Karadag, Y. Koc, M. Turan, M. Ozturk, A comparative study of linear and non-linear regression analysis for ammonium exchange by clinoptilolite zeolite, J. Hazard. Mater., 144 (2007) 432–437.

[9] S. Lagergren, Zur theories der sogenannten adsorption gel6ster stoffe, Kungliga Svenska Vetenskapsakademiens, Handlingar, 24 (1898) 1–39.

[10] H.H.M. Darweesh, Ceramic wall and floor tiles containing local waste of cement kiln dust-Part II: dry and firing shrinkage as well as mechanical properties, Am. J. Civ. Eng. Arch., 4 (2016) 44–49.

[11] R.A. Donat, A. Akdogan, E. Erdem, H. Cetisli, Thermodynamics of Pb^{2+} and Ni^{2+} adsorption onto natural bentonite from aqueous solutions, J. Colloid Interface Sci., 286 (2005) 43–52.

[12] Y.-T. Huang, L.-C. Lee, M.-C. Shih, A study on the pseudo-second-order kinetic equation for the adsorption of methylene blue onto nitric acid-treated rice husk comparison of linear methods, Int. J. Sci. Res. Publ. (IJSRP), 8 (2018) 509–515.

[13] N. Onursal, M.C. Dal, Altı tip yalancı-ikinci dereceli (Ho–McKay) kinetik denkleminin malahit yeşilinin Siirt Kurtalan/Ağaçlıpınar kili ile adsorpsiyonunda karşılaştırılmalı doğrusal yöntemler, Internetional Siirt Scıentific Research Congress, Siirt/Turkey, 2021 (Comparative Linear Methods in the Adsorption of Malachite Green with Siirt Kurtalan/Ağaçlıpınar Clay of Six Types of Pseudo-Second-Order (Ho–McKay) Kinetic Equations, International Siirt Scientific Research Congress, Siirt/Turkey, 2021).

[14] D. Jiang, Y. Yang, C. Huang, M. Huang, J. Chen, T. Rao, X. Ran, Removal of the heavy metal ion nickel(II) via an adsorption method using flower globular magnesium hydroxide, J. Hazard. Mater., 373 (2019) 131–140.

[15] N. Onursal, Ö. Yavuz, A.R. Kul, Pb(II) iyonlarının aktive edilmemiş karışık tipteki kil ile sudan uzaklaştırılması, Anadolu Kongreleri 3. Uluslararası Uygulamalı Bilimler Kongresi, Diyarbakır: ubak yayınevi, 2018, pp. 626–657. (Removal of Pb(II) Ions From Water with Unactivated Mixed Type Clay, ICNASEN, Diyarbakır: Ubak Publishing House, 2018, pp. 626–657).

[16] T. Özdemir, Nitratın çeşitli topraklardaki adsorpsiyon ve taşınımının incelenmesi, (TJTS) Elazığ, 2006. (Investigation of Adsorption and Transport of Nitrate in Various Soils, (TJTS), Elazig, 2006).

[17] A. Nimibofa, A.N. Ebelegi, D. Wankasi, Modelling and ınterpretation of adsorption ısotherms, J. Chem., (2017) 1–11, doi: 10.1155/2017/3039817.

[18] S. Kalam, S.A. Abu-Khamsin, M.S. Kamal, S. Patil, Surfactant adsorption ısotherms: a review, ACS Omega, 6 (2021) 32342–32348, doi: 10.1021/acsomega.1c04661.

[19] A.M.S. Khairul, Z.I. Nor, L.J. Ramizah, M.A. Nurul Ain, M.S. Norsuzailina, G.G. Genevieve, B. Rubiyah, S.A. Zauzi, N. Syuhada, Application of Freundlich and Temkin ısotherm to study the removal of Pb(II) via adsorption on activated carbon equipped polysulfone membrane, Int. J. Eng. Technol., 7 (2018) 91–93.

[20] D.A. Hanaor, M. Ghadiri, W. Chrzanowski, Y. Gan, Scalable surface area characterization by electrokinetic analysis of complex anion adsorption, Langmuir, 30 (2014) 15143–15152, doi: 10.1021/la503581e.

[21] N. Onursal, M.C. Dal, A.R. Kul, Ö. Yavuz, Cu(II) iyonlarının doğal karışık tipteki kil ile sulu ortamdan uzaklaştırılması, izoterm, kinetik ve termodinamik parametrelerin incelenmesi, (Removal of Cu(II) ions from the aqueous medium with natural mixed type clay, investigation of isotherm, kinetic and thermodynamic parameters), Euroasia J. Math. Eng. Nat. Med. Sci., (2020) 85–103. Available at: https://euroasiajournal.org/index.php/ejas/article/view/42/40
[22] M.C. Dal, Cu(II), Ni(II) ve Co(II)'nin Karacadağ skoryası ile adsorpsiyonunun izoterm, kinetik ve termodinamik analizi, Dicle Ünivesitesi Fen Bilimleri Enstitüsü,doktora tezi, Diyarbakır, 2021. (Isotherm, Kinetic and Thermodynamic Analysis of the Adsorption of Cu(II), Ni(II) and Co(II) with Karacadağ Score, DUINAS, Doctoral Dissertation, Diyarbakır, 2021).
[23] M. Karimi, M.H. Entezari, M. Chamsaz, Sorption studies of nitrate ion by a modified beet residue in the presence and absence of ultrasound, Ultrason. Sonochem., 17 (2010) 711–717.
[24] A.R. Kul, A. Aldemir, H. Koyuncu, An investigation of natural and modified diatomite performance for adsorption of basic Blue 41: isotherm, kinetic, and thermodynamic studies, Desal. Water Treat., 229 (2021) 384–394.
[25] M.S. Sajab, C.H. Chia, S. Zakaria, S.M. Jani, M.K. Ayob, K.L. Chee, P.S. Khiew, W.S. Chiu, Citric acid modified kenaf core fibres for removal of methylene blue from aqueous solution, Bioresour. Technol., 102 (2011) 7237–7243.
[26] S. Sahoo, Uma, S. Banerjee, Y.C. Sharma, Application of natural clay as a potential adsorbent for the removal of a toxic dye from aqueous solutions, Desal. Water Treat., 52 (2013) 6703–6711.
[27] T. Wajima, Synthesis of Fe-layered double hydroxide from bittern and its nitrate-ion removal ability, Clay Miner., 56 (2021) 65–74.
[28] A.M. Aljeboree, A.N. Alshirifi, A.F. Alkaim, Kinetics and equilibrium study for the adsorption of textile dyes on coconut shell activated carbon, Arabian J. Chem., 10 (2017) S3381–S3393.
[29] M.A. El-Nemr, M. Yılmaz, S. Ragab, A. El Nemr, Biochar-so prepared from pea peels by dehydration with sulfuric acid improves the adsorption of Cr^{6+} from water, Biomass Convers. Biorefin., (2022), doi: 10.1007/S13399-022-02378-4.